

# Adaptive Attention-Based Model for 5G Radio-based Outdoor Localization

Ilayda Yaman\*, Guoda Tian\*, Fredrik Tufvesson\*, Ove Edfors\*, Zhengya Zhang<sup>†</sup>, Liang Liu\*

\*Dept. of Electrical and Information Technology, Lund University, Sweden

<sup>†</sup>Department of Electrical Engineering and Computer Science, University of Michigan, Ann Arbor, USA

**Abstract**—Radio-based localization in dynamic environments, such as urban and vehicular settings, requires systems that can efficiently adapt to varying signal conditions and environmental changes. Factors such as multipath interference and obstructions introduce different levels of complexity that affect the accuracy of the localization. Although generalized models offer broad applicability, they often struggle to capture the nuances of specific environments, leading to suboptimal performance in real-world deployments. In contrast, specialized models can be tailored to particular conditions, enabling more precise localization by effectively handling domain-specific variations and noise patterns. However, deploying multiple specialized models requires an efficient mechanism to select the most appropriate one for a given scenario. In this work, we develop an adaptive localization framework that combines shallow attention-based models with a router/switching mechanism based on a single-layer perceptron (SLP). This enables seamless transitions between specialized localization models optimized for different conditions, balancing accuracy, computational efficiency, and robustness to environmental variations. We design three low-complex localization models tailored for distinct scenarios, optimized for reduced computational complexity, test time, and model size. The router dynamically selects the most suitable model based on real-time input characteristics. The proposed framework is validated using real-world vehicle localization data collected from a massive MIMO base station (BS), demonstrating its ability to seamlessly adapt to diverse deployment conditions while maintaining high localization accuracy.

**Index Terms**—Vehicle localization, radio-based localization, adaptive models, attention-based models

## I. INTRODUCTION

Reliable and accurate location information with low latency is essential to ensure efficient and reliable workflows in various tasks, including vehicle navigation, intelligent traffic management, and autonomous driving. Localization in urban environments presents significant challenges due to multipath propagation, signal blockages, and dynamic environmental conditions. Traditional Global Navigation Satellite System (GNSS)-based positioning often suffers from degraded accuracy in dense urban areas, where buildings and other structures obstruct satellite signals. A robust and continuously available localization solution is needed that works seamlessly across different environments and platforms [1]. For example, in [2], the authors implement random forest and gradient boosting algorithms to effectively use multipath information to improve outdoor location. When tested on real-world data, machine learning (ML) models achieve a mean localization error of approximately 100 m in an area of 580,000 m<sup>2</sup>.

A key challenge in radio-based localization is designing computationally efficient models capable of adapting to dynamic signal conditions. Several works in the literature have considered using massive multiple-input-multiple-output (MIMO) technologies together with ML methods to achieve robust, low-latency localization in diverse scenarios [3]–[5]. A widely adopted approach is fingerprinting, where channel state information or channel impulse response (CIR) measurements serve as unique signatures of specific locations within an environment. By collecting and storing these measurements in a database, ML models can be trained to map real-time channel responses to their corresponding spatial coordinates  $(x, y)$ . Deep learning-based fingerprinting methods have demonstrated high localization accuracy by taking advantage of the spatial and temporal characteristics of the wireless channel [6]–[8].

Specialized fine-tuned models can achieve higher accuracy with smaller model sizes and less computational complexity compared to generalized models. To accommodate multiple conditions, general models are more complex, use more parameters, and have higher test times and computational costs. However, to fully leverage the advantages of specialized models across diverse environments, a router is needed to dynamically determine which model is best suited for a given scenario. By analyzing input characteristics and environmental conditions, the router selects the most appropriate specialized model, ensuring that only the necessary parameters are activated at each time step. Due to the continuous nature of the application, switching between different models would happen rarely, and the weights would be reused extensively. Thus, the computational overhead is reduced and high localization accuracy is maintained under different conditions. By integrating adaptive models, localization systems dynamically adjust to varying urban scenarios, ensuring reliable and efficient positioning for applications such as autonomous driving, intelligent transportation, and urban navigation.

Fig. 1 visualizes three methods, with Method 1 being the most general and Method 3 the most specialized. Method 1 uses the same trainable parameters and architecture in all data subsets. Method 2 consists of  $N$  sets of trainable parameters that are loaded into the same model depending on the selected subset of data. Switching between trainable parameters is done manually. The proposed adaptive model, Method 3, includes specialized trainable parameters and a model architecture with

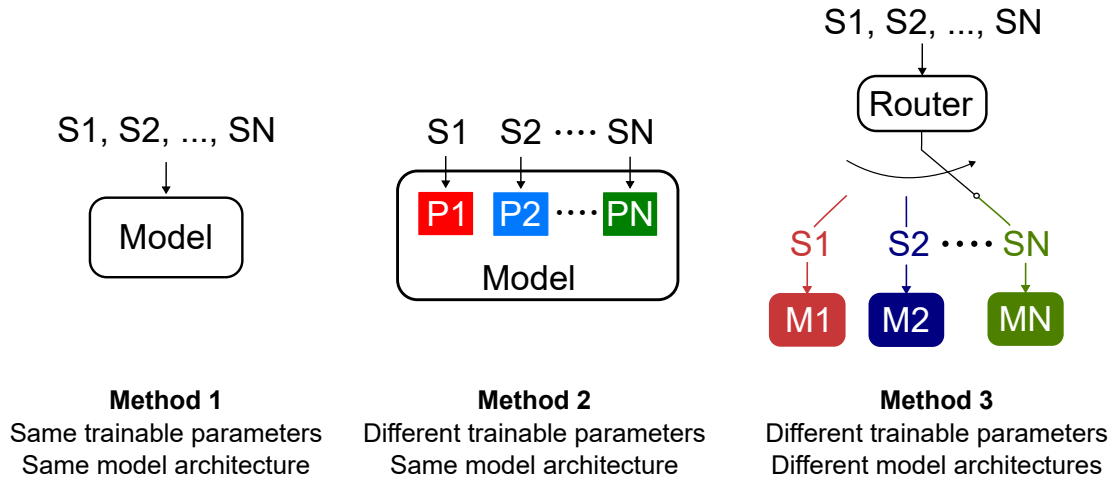


Fig. 1: Overview of the adaptive model, where S, N, P, and M represent the subset of data, the total number of subsets, the trainable parameters (weights and biases), and the model, respectively

run-time adaptation between different data subsets. The router in Method 3 determines which scenario the given input belongs to and selects the appropriate model accordingly, ensuring that only a subset of all parameters is active.

By tuning the model architecture parameters, the specialized models provide better localization accuracy than the other methods. The number of active trainable parameters and the training and testing times are also reduced. The main contributions of the paper are:

- We establish specialized attention-based models to minimize computational complexity, localization error, and model size for different scenarios. We then compare the results with more general models.
- We develop an adaptive localization framework capable of dynamically adjusting to environmental changes and signal propagation conditions. Measurement data from a massive MIMO base station (BS) and a moving user equipment (UE) on a vehicle is used for verification.

## II. FUNDAMENTALS OF ATTENTION MODELS AND EXPERIMENTAL VALIDATION

This section provides an overview of the key components of attention-based models and describes the measurement campaign conducted to validate the proposed model.

### A. Building Blocks of Attention-based Models

The architecture of the shallow encoder-only attention-based model is shown in Fig. 2. The model consists of positional encoding, multihead attention, and feedforward layers, each followed by residual connections and optional layer normalization. Additionally, a pooling layer is applied before the fully connected neural network (FCNN) to reduce model size.

1) *Positional Encoding*: is used to incorporate position information into the model, using sinusoidal positional encoding. This encoding method ensures that position information is embedded in a continuous and differentiable manner, allowing

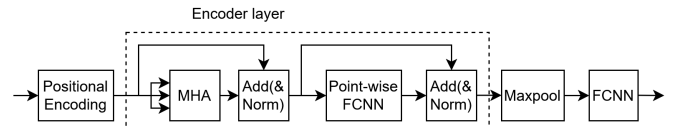


Fig. 2: The attention-based algorithm pipeline with one encoder layer and pooling layer added.

the model to capture relative positional relationships effectively. The use of different frequency scales helps the model generalize to unseen sequence lengths and improves its ability to encode sequential dependencies.

2) *Multi-Head Attention (MHA)*: is the fundamental mechanism in attention-based architectures, enabling efficient parallel processing of input data [9]. It builds on Scaled Dot-Product Attention, which computes attention scores based on query, key, and value matrices derived from the input tensor  $\mathbf{X} \in \mathbb{R}^{d_k \times d_{\text{model}}}$  at a given timestep

$$\mathbf{Q} = \mathbf{X} \mathbf{W}_q, \mathbf{K} = \mathbf{X} \mathbf{W}_k, \mathbf{V} = \mathbf{X} \mathbf{W}_v. \quad (1)$$

The attention mechanism is computed as

$$\text{Attention}(\mathbf{Q}, \mathbf{K}, \mathbf{V}) = \text{softmax} \left( \frac{\mathbf{Q} \mathbf{K}^T}{\sqrt{d_k}} \right) \mathbf{V}, \quad (2)$$

where  $d_k$  is the dimensionality of the key vectors, and the scaling factor  $\sqrt{d_k}$  prevents large softmax values that could hinder training. The MHA extends this by applying multiple attention mechanisms in parallel, each with different learned projections

$$\text{head}_i = \text{Attention}(\mathbf{Q} \mathbf{W}_i^Q, \mathbf{K} \mathbf{W}_i^K, \mathbf{V} \mathbf{W}_i^V), \quad (3)$$

where  $\mathbf{W}_i^Q, \mathbf{W}_i^K, \mathbf{W}_i^V$  are learned projection matrices for the  $i$ -th attention head. The outputs of all heads are concatenated and projected to obtain the final representation:

$$\text{MHA}(\mathbf{Q}, \mathbf{K}, \mathbf{V}) = \text{Concat}(\text{head}_1, \dots, \text{head}_h) \mathbf{W}^O, \quad (4)$$

where  $h$  is the number of attention heads, and  $\mathbf{W}^O$  is a learned output projection matrix. By allowing the model to attend to different representation subspaces simultaneously, MHA enhances its ability to capture complex dependencies, e.g. in challenging environments where noise and signal multipath effects complicate traditional methods.

3) *Layer Normalization (LN)*: normalizes activations across the feature dimension for each input independently, making it effective for stabilizing deep networks.

4) *Position-wise Feed-Forward Networks (FFN)*: applies two linear transformations with an activation function in between. Each token in the sequence is processed independently through a position-wise transformation. The dimensionality of the inner layer is represented as  $d_{\text{ff}}$ . The activation function is the rectified linear unit (ReLU).

5) *Pooling layer*: reduces the model size and computational complexity while maintaining key feature representations, a one-dimensional maximum pooling layer is introduced between the encoder layer and the FCNN. Padding can be added to adjust alignment. This approach effectively decreases the number of parameters and computations required in subsequent layers, leading to a more compact and efficient model.

6) *Dropout*: is a regularization technique that helps prevent overfitting by randomly deactivating neurons during training.

## B. Experiments

The measurement campaign is based on a commercial self-contained massive MIMO BS and a single moving user in a vehicle. The vehicle is equipped with a UE and a GNSS receiver, which is used for ground truth. The BS operates at 3.85 GHz center frequency and has 100 MHz bandwidth.

The BS is equipped with 32 vertically and 32 horizontally polarized antenna ports. The transmitter/receiver antenna elements are used to form 64 beams in both the downlink (DL) and the uplink (UL). The UL data from 2 UE antenna ports and 46 subcarriers are selected to be recorded by the BS. The 32 horizontal and vertical beam space matrices of the channel transfer function (CTF) of the 1st and 2nd antenna ports for the time  $t$  and 46 subcarriers are defined as  $\mathbf{H}_{V1,t}$ ,  $\mathbf{H}_{H1,t}$ ,  $\mathbf{H}_{V2,t}$  and  $\mathbf{H}_{H2,t}$ , respectively. The combined channel matrix corresponds to  $\mathbf{H}_t \in \mathbb{C}^{128 \times 46} = [\mathbf{H}_{H1,t}^T, \mathbf{H}_{V1,t}^T, \mathbf{H}_{H2,t}^T, \mathbf{H}_{V2,t}^T]^T$ . The data is pre-processed to compute the CIR beam matrix, which is then used as input to the model.

The UE is mounted on a vehicle following three trajectories, forming three scenarios, shown by yellow lines in Fig. 3. The average speed of the vehicle is 15 km/h and the BS is mounted on a 20-meter-high building. The vehicle follows the given trajectories for five laps. For more detailed information on the measurement campaign, see [3].

In the first scenario, the vehicle is driving on the roof of a garage which is approximately 10 meters above the ground level, and follows a trajectory that mostly captures line-of-sight (LoS) conditions. The second scenario is at the ground level below the BS, and the vehicle is mostly not on direct LoS from the BS. Lastly, in the third scenario, which takes place at ground level, the LoS between the vehicle and the BS is

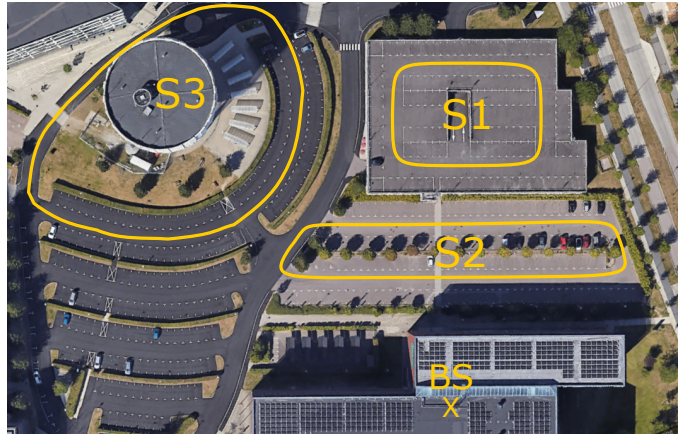


Fig. 3: Bird-eye view of the measurement environment and trajectories labeled S1, S2, and S3.

intermittently visible along the trajectory, with some sections being obstructed by the tower seen in Fig. 3. We select these three scenarios as our three subsets of data, S1, S2, and S3.

## C. Evaluation Method

Of the five laps, the first four laps are used for training and validation, whereas the fifth lap of each scenario is reserved for testing. For the generalized model, the training/validation datasets of different scenarios are randomly mixed to create a dataset that consists of different scenarios, whereas the specialized models are only trained on the specific trajectories.

The accuracy of the localization algorithms is calculated using the mean of the Euclidean distance between the estimated locations and the ground truth labels. Mean Euclidean Error (MEE) is defined as

$$\text{MEE} = \frac{1}{N} \sum_{i=1}^N \|\hat{\mathbf{y}}_i - \mathbf{y}_i\|_F \quad (5)$$

where  $N$ ,  $\hat{\mathbf{y}}_i$  and  $\mathbf{y}_i$  represent the number of samples, predicted 2D locations and the ground truth labels, respectively.  $\|\cdot\|_F$  is the Frobenius norm.

## III. PROPOSED MODEL

The model architecture selection of specialized models and the router that is used to dynamically switch between different scenarios are described in this section. The hyperparameter configuration of the model is summarized in Table I.

### A. Specialized models

The complexity of model design is closely linked to the characteristics of the channel state information, which is highly influenced by multipath propagation. In a non LoS (NLoS) environment, the CIR and angular characteristics would differ significantly from a scenario where there is a dominant LoS component. In LoS environments, the energy is typically concentrated in the LoS path; therefore, the power delay profile changes slowly with UE movement. For example, in Fig. 4, the power is concentrated in the few early delay bins. The

TABLE I: Hyperparameters of the model.

Parameter	Value
Epochs	200
Batch Size (b)	64
$d_{\text{model}}$	46
$d_k$	128
$d_{\text{ff}}$	64
Learning Rate	0.0006
Number of heads	2
Dropout Rate	0.05
Loss function	MSE

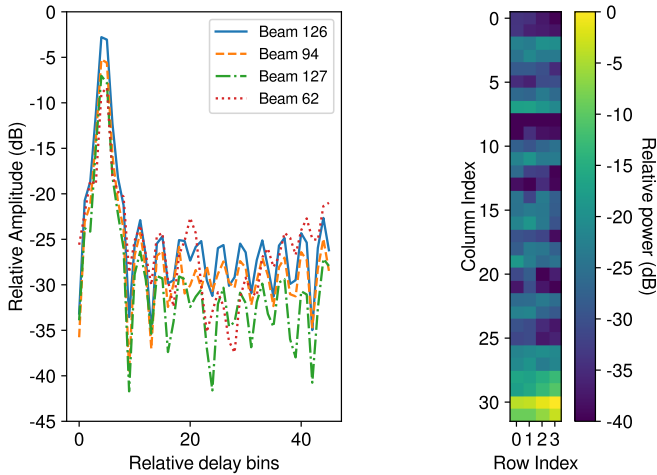


Fig. 4: Power delay profile of the 4 dominant beams and relative power of all 128 beams in a LoS scenario.

relative power of each beam is calculated by summarizing the power among all delay bins.

In highly rich scattering environments (e.g., dense urban areas, indoor clutter), multipath reflections come from many uncorrelated scatterers, leading to less structured, more random multipath components. An example is presented in Fig. 5, showing the power delay profile and the corresponding beam matrix (the angular characteristics) in an urban NLoS environment. Unlike LoS, the power delay profile varies quickly with different UE positions in challenging urban NLoS scenarios. Therefore, it is worth designing a different model to better handle the swift changes of channel features. Deeper models can capture complex multipath interactions in NLoS or dense urban environments, while for LoS scenarios, simpler models are sufficient.

The following model architecture parameters are explored to select specialized models for different scenarios with different complexities: the effect of increasing the number of encoder layers from 1 to 5, removing/adding layer normalization, and adding a pooling layer before the FCNN layer. The pooling layer downsamples the input to the FCNN layer by selecting the maximum value in non-overlapping segments of size 4. Padding is added to adjust the alignment. The output dimension becomes  $(b, d_k, (d_{\text{model}} + 2)/4)$ , resulting in a reduced number of trainable parameters. By exploring

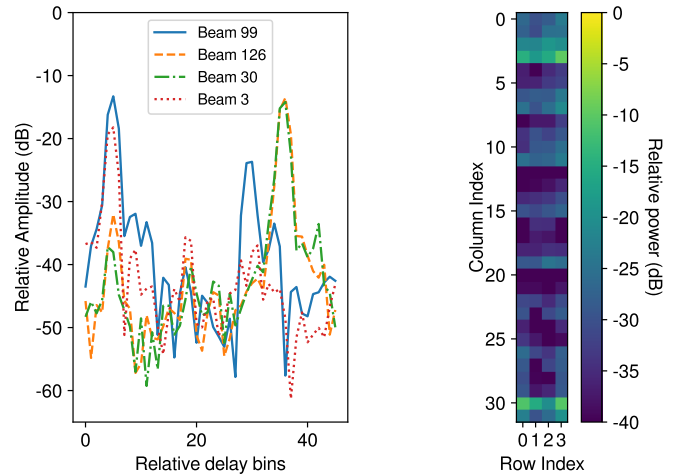


Fig. 5: Power delay profile of the 4 dominant beams and relative power of all 128 beams in an NLoS scenario.

these parameters and comparing them to Method 1, the optimal specialized models are selected that improve the accuracy of the model while keeping the size of the model similar for each scenario.

The results are shown in Table II, comparing the generalized (Method 1) and specialized (Method 3) models. The highest localization accuracy for Method 1 is achieved when using 3 encoder layers, resulting in MEE of (0.47m, 0.83m, 0.81m) for S1, S2, and S3, respectively. The best results are achieved when layer normalization is added for S3 and removed for S1 and S2. For Model 3, a lower MEE for S1 can be achieved by using 1 encoder layer, with or without the addition of pooling and layer normalization. For S2 and S3, 2 encoder layers are needed to achieve better performance with specialized models. Although adding more encoder layers can further reduce the MEE, the computational complexity and model size increase accordingly.

### B. Router

In the proposed model, the router determines the type of scenario based on the input, a task known as classification. ML classifiers such as the Single-Layer Perceptron (SLP), Multi-layer Perceptron (MLP), and Convolutional Neural Networks (CNN) are widely used for classification tasks. Among SLP, MLP, and CNN, the SLP is the simplest and least computationally expensive, making it suitable for linearly separable problems. It consists of an input layer directly connected to an output layer, with no hidden layers in between. The SLP performs a linear transformation of the input and applies an activation function to produce the output, and defined as

$$\mathbf{y} = \sigma(\mathbf{x}W + b) \quad (6)$$

where  $\mathbf{x} \in \mathbb{R}^n$  is the input vector,  $W$  is the weight vector,  $b$  is the bias term,  $\sigma(\cdot)$  is the activation function (typically sigmoid or softmax), and  $\mathbf{y}$  is the predicted output. The training and

TABLE II: The localization accuracy of Method 1 and Method 3 for different model architectures (dropout = 0.05, EL = Number of Encoder Layers, LN = Layer Normalization, MP = maxpool).

EL	LN	MP	MEE (m), Specialized			MEE (m), Generalized		
			S1	S2	S3	S1	S2	S3
1	-	-	0.41	0.96	0.99	0.85	1.14	1.11
2	-	-	0.40	0.80	0.93	0.53	0.95	1.00
3	-	-	0.35	0.81	0.83	<b>0.47</b>	<b>0.83</b>	0.86
4	-	-	0.33	0.80	0.60	0.51	1.02	0.86
5	-	-	0.49	6.16	0.59	1.47	3.10	2.28
1	+	-	0.45	1.06	0.97	0.69	1.18	0.97
2	+	-	0.37	0.88	0.74	0.54	1.00	1.05
3	+	-	0.37	0.71	0.77	0.55	0.86	<b>0.81</b>
4	+	-	0.34	0.80	0.65	0.60	0.98	0.76
5	+	-	1.60	5.76	1.01	0.68	1.08	0.97
1	-	+	<b>0.40</b>	1.10	1.26	0.93	1.80	1.62
2	-	+	0.38	<b>0.78</b>	<b>0.77</b>	0.64	1.14	1.24
3	-	+	0.38	0.81	0.81	0.57	1.14	1.11
4	-	+	0.40	0.93	1.55	0.88	1.30	1.13
5	-	+	9.68	0.79	2.62	2.59	4.39	3.91
1	+	+	0.61	1.10	1.25	1.13	1.57	1.84
2	+	+	0.37	0.89	0.75	0.76	1.20	1.03
3	+	+	0.38	0.92	0.82	0.70	1.08	1.10
4	+	+	0.33	0.99	0.97	0.75	1.15	0.88
5	+	+	0.86	7.84	3.00	1.13	1.93	1.74

test data split used for the attention-based model is also applied to the SLP model.

When the router is implemented as an MLP or CNN, it achieves a test accuracy of 100%. To investigate the effects of overfitting, the dropout is increased to 0.7, and a weight decay of  $1 \times 10^{-5}$  is introduced. As a result, the test accuracy decreases to 99%. These findings indicate that the router model can be further reduced in complexity, potentially to an SLP.

With the full input matrix, the training and validation losses of the SLP model converge to zero, and the test accuracy remains at 100%. To explore further model compression, trials are conducted using a smaller model that trains on the beam power matrix of one relative delay bin. The corresponding input is fed into a compact model with 387 parameters, achieving a test accuracy of 98.87%. Additional trials across different relative delay bins reveal that the minimum observed test accuracy is 97.76%. Given that there are 46 relative delay bins in total, this shows that using a subset of input features can still produce high classification accuracy.

#### IV. RESULTS

The final proposed architecture is depicted in Fig. 6. The diagram illustrates the active model with black lines, while the inactive models appear in gray.

Table III summarizes the final results obtained for the three methods: Method 1 (the generalized model), Method 2 (different trainable parameters of each model but the same model architecture [3]), and Method 3 (the proposed adaptive model). The comparison is based on various metrics, including MEE in three scenarios (S1, S2, and S3), the number of model

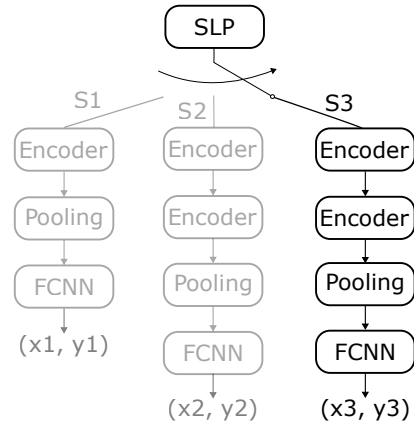


Fig. 6: The final block diagram of the proposed method after the selection of the specialized models and the SLP router. For clarity, the positional encoding is not shown.

parameters, adaptivity, and test time for S1. Test time is provided as a reference and may vary depending on the underlying hardware, software environment, and implementation details. All experiments are carried out in a Linux-based CPU-only environment with 64 GB of RAM.

TABLE III: Final result comparison.

	Method 1	Method 2 [3]	Method 3
S1, MEE (m)	0.47	0.99	0.40
S2, MEE (m)	0.83	2.00	0.78
S3, MEE (m)	0.86	1.01	0.77
number of parameters <sup>a</sup>	303k	227k + 227k + 227k	87k + 126k + 126k
adaptive	+	-	+
test time, S1 (s)	4.40	1.83	1.48

<sup>a</sup> Only one subset of the parameters is active at a given time for Method 2 and 3.

In [3], the accuracy of Method 2 is given as 0.99 m, 2.00 m, and 1.01 m for S1, S2, and S3, respectively. In comparison, the proposed method shows improved accuracy, achieving MEE of 0.40 m, 0.78 m, and 0.77 m for S1, S2, and S3, respectively. Method 1, which is the generalized model, achieves an MEE of 0.47 m, 0.83 m, and 0.86 m for S1, S2, and S3, respectively, showing a slightly lower performance than the proposed method. The router system enables the activation of a single model at any moment, reducing the number of active parameters by 58% to 71% and test time by 66%, compared to the generalized model. The test time of the router is negligible. Please note that these results are specific to the given dataset, and adaptations may be needed for different deployment scenarios.

#### V. CONCLUSION

In this work, we present an adaptive localization model that dynamically selects specialized sub-models based on the given input scenario. We compare our approach against two methods: (i) a manually switched model where each scenario is assigned to a specialized model, and (ii) a generalized model

that attempts to handle all scenarios with a single model but suffers from degraded localization accuracy. The proposed model uses a routing mechanism to determine whether an input belongs to S1, S2, or S3, activating the corresponding sub-model accordingly. This approach enables the use of only a subset of the total parameters at any given time, reducing computational complexity compared to the generalized model, while achieving higher accuracy. To further improve efficiency, we introduce a pooling layer and remove layer normalization, reducing the model size and computational cost. These results highlight the potential of adaptive computation in radio-based localization, balancing accuracy and computational complexity across varying environmental conditions.

#### ACKNOWLEDGMENT

The authors would like to thank Jens Gulin and Axel Berg from Lund University, as well as Wei Tang, Sangbu Yun, and the Lab for Efficient Application Processors (LEAPs) at the Department of Electrical Engineering and Computer Science, University of Michigan, Ann Arbor, for their valuable suggestions regarding our paper. This work is funded by the Swedish Research Council, Ericsson AB, and ELLIIT (Excellence Center at Linköping-Lund in Information Technology).

#### REFERENCES

- [1] S. Djosic, I. Stojanovic, M. Jovanovic, and G. L. Djordjevic, "Multi-algorithm UWB-based localization method for mixed LOS/NLOS environments," *Computer Communications*, vol. 181, pp. 365–373, 2022.
- [2] M. N. de Sousa, R. Sant'Ana, R. P. Fernandes, J. C. Duarte, J. A. Apolinário, and R. S. Thomä, "Improving the performance of a radio-frequency localization system in adverse outdoor applications," *EURASIP J. Wirel. Commun. Netw.*, vol. 2021, May 2021.
- [3] G. Tian, D. Pjanić, X. Cai, B. Bernhardsson, and F. Tufvesson, "Attention-Aided Outdoor Localization in Commercial 5G NR Systems," *IEEE Transactions on Machine Learning in Communications and Networking*, vol. 2, pp. 1678–1692, 2024.
- [4] A. Sellami, L. Nasraoui, and L. N. Atallah, "Multi-Stage Localization for Massive MIMO 5G Systems," in *2020 IEEE 91st Vehicular Technology Conference (VTC2020-Spring)*, pp. 1–6, 2020.
- [5] A. Decurninge, L. G. Ordóñez, P. Ferrand, H. Gaoning, L. Bojje, Z. Wei, and M. Guillaud, "CSI-based Outdoor Localization for Massive MIMO: Experiments with a Learning Approach," in *2018 15th International Symposium on Wireless Communication Systems (ISWCS)*, pp. 1–6, 2018.
- [6] A. Al-Tahmeesschi, J. Talvitie, M. López-Benítez, and L. Ruotsalainen, "Deep Learning-based Fingerprinting for Outdoor UE Positioning Utilising Spatially Correlated RSSs of 5G Networks," in *2022 International Conference on Localization and GNSS (ICL-GNSS)*, pp. 1–7, 2022.
- [7] G. Tian, I. Yaman, M. Sandra, X. Cai, L. Liu, and F. Tufvesson, "Deep-learning based high-precision localization with massive MIMO," *IEEE Transactions on Machine Learning in Communications and Networking*, 2023.
- [8] R. Whiton, J. Chen, T. Johansson, and F. Tufvesson, "Urban Navigation with LTE using a Large Antenna Array and Machine Learning," in *2022 IEEE 95th Vehicular Technology Conference: (VTC2022-Spring)*, pp. 1–5, 2022.
- [9] A. Vaswani, N. Shazeer, N. Parmar, J. Uszkoreit, L. Jones, A. N. Gomez, L. Kaiser, and I. Polosukhin, "Attention is all you need," in *Proceedings of the 31st International Conference on Neural Information Processing Systems, NIPS'17*, (Red Hook, NY, USA), pp. 6000–6010, Curran Associates Inc., 2017.